Supplemental Materials and Methods

Data analysis and Softwares

RNA-Seq. All RNA-Seq datasets, whether specifically generated for this study or obtained from public databases (see Data availability paragraph of the Materials and Methods section in the main text), have been analyzed/re-analyzed using the same pipeline implemented for this project. The RNA-seq data was analyzed using the Galaxy platform (The Galaxy Community et al., 2022). HTSeq (Anders et al., 2015) mapped the reads to the GRCm38 assembly for mouse and GENCODE-M25 (www.gencodegenes.org) was used to count the transcript abundance. Differential expression analysis was done *via* the DESeq2 (Love et al., 2014) package for R, which uses the Wald test for significance. To define the transcriptional signatures of activated B cells, PBs, and PCs, the analysis was performed using the naïve B cell RNA-Seq dataset from the same study (Minnich et al., 2016) for baseline comparison. Expression of differentially expressed genes were obtained from Immgen database (The Immunological Genome Project et al., 2020) and visualize by R and ggolot2 packages (https://ggplot2.tidyverse.org/) after scaling. For the comparative assessment of $Cd19^{Cre/+}$ and $Rif1^{F/F}Cd19^{Cre/+}$ B cell transcriptomes at 48 h after activation, RNA-seq datasets from L-I and L-B-T splenocytes cultures were merged. The increase in sample size (from 3 to 6 repeats) for both groups enhanced statistical power to detect minor gene expression differences. The multiple treatments are used to discern genotype effects, thus ensuring that the observed differences are due to the absence of RIF1.

ChIP-Seq. ChIP-Seq and BLIMP1 Bio-ID datasets (see Data availability paragraph) have been analyzed/re-analyzed using the same pipeline implemented for this project. FASTQ files were aligned against mouse genome (mm10) using BWA aligner (Li & Durbin, 2009). Processing and peak-calling of ChIP-Seq data were performed with MACS2 (Zhang et al., 2008). Peak annotation was done using R and ChIPseeker package (Yu et al., 2015). Functional assessment of genomic regions enrichment and motif analysis were performed by GREAT and MEME-ChIP, respectively (Machanick & Bailey, 2011; McLean et al., 2010). For the comparative genomic distribution analysis of RIF1, H3K4me3, and H3K27me3 in reference to BLIMP1-occupied regions, the aligned reads were converted into BigWig format. The signals were subsequently transformed into a matrix *via* the ComputeMatrix software, and visualized as a heatmap (Ramírez et al., 2016).

Statistical analysis. The statistical significance of differences between groups was determined by the Mann–Whitney U test for all data presented in this study, with the following exceptions. For the RNA-Seq analysis, the expression values of specific transcripts were normalized by DESeq2, and genes with an adjusted p-value < 0.05 were considered to be significantly differentially expressed. Statistical details of experiments can be also found in the figure legends.

Source Codes for Data Analysis. All codes used to generate graphs and to compare different datasets can be found on our GitHub page (https://github.com/arahjou/RIF1_paper).

References:

Anders, S., Pyl, P. T., & Huber, W. (2015). HTSeq—A Python framework to work with high-throughput sequencing data. *Bioinformatics (Oxford, England)*, *31*(2), 166–169. https://doi.org/10.1093/bioinformatics/btu638

Li, H., & Durbin, R. (2009). Fast and accurate short read alignment with Burrows-Wheeler transform. *Bioinformatics (Oxford, England)*, *25*(14), 1754–1760. https://doi.org/10.1093/bioinformatics/btp324

Love, M. I., Huber, W., & Anders, S. (2014). Moderated estimation of fold change and dispersion for RNA-seq data with DESeq2. *Genome Biology*, *15*(12), 550. https://doi.org/10.1186/s13059-014-0550-8

Machanick, P., & Bailey, T. L. (2011). MEME-ChIP: Motif analysis of large DNA datasets. *Bioinformatics*, *27*(12), 1696–1697. https://doi.org/10.1093/bioinformatics/btr189

McLean, C. Y., Bristor, D., Hiller, M., Clarke, S. L., Schaar, B. T., Lowe, C. B., Wenger, A. M., & Bejerano, G. (2010). GREAT improves functional interpretation of cis-regulatory regions. *Nature Biotechnology*, *28*(5), 495–501. https://doi.org/10.1038/nbt.1630

Minnich, M., Tagoh, H., Bönelt, P., Axelsson, E., Fischer, M., Cebolla, B., Tarakhovsky, A., Nutt, S. L., Jaritz, M., & Busslinger, M. (2016). Multifunctional role of the transcription factor Blimp-1 in coordinating plasma cell differentiation. *Nature Immunology*, *17*(3), 331–343. https://doi.org/10.1038/ni.3349

Ramírez, F., Ryan, D. P., Grüning, B., Bhardwaj, V., Kilpert, F., Richter, A. S., Heyne, S., Dündar, F., & Manke, T. (2016). deepTools2: A next generation

web server for deep-sequencing data analysis. *Nucleic Acids Research*, *44*(W1), W160–W165. https://doi.org/10.1093/nar/gkw257

The Galaxy Community, Afgan, E., Nekrutenko, A., Grüning, B. A., Blankenberg, D., Goecks, J., Schatz, M. C., Ostrovsky, A. E., Mahmoud, A., Lonie, A. J., Syme, A., Fouilloux, A., Bretaudeau, A., Nekrutenko, A., Kumar, A., Eschenlauer, A. C., DeSanto, A. D., Guerler, A., Serrano-Solano, B., … Briggs, P. J. (2022). The Galaxy platform for accessible, reproducible and collaborative biomedical analyses: 2022 update. *Nucleic Acids Research*, *50*(W1), W345–W351. https://doi.org/10.1093/nar/gkac247

The Immunological Genome Project, Aguilar, S. V., Aguilar, O., Allan, R., Amir, E. A. D., Angeli, V., Artyomov, M. N., Asinovski, N., Astarita, J., Austen, K. F., Bajpai, G., Barrett, N., Baysoy, A., Benoist, C., Bellemare-Pelletier, A., Berg, B., Best, A., Bezman, N., Blair, D., … Ziemkiewicz, C. (2020). ImmGen at 15. *Nature Immunology*, *21*(7), 700–703. https://doi.org/10.1038/s41590-020-0687-4

Yu, G., Wang, L.-G., & He, Q.-Y. (2015). ChIPseeker: An R/Bioconductor package for ChIP peak annotation, comparison and visualization. *Bioinformatics*, *31*(14), 2382–2383. https://doi.org/10.1093/bioinformatics/btv145

Zhang, Y., Liu, T., Meyer, C. A., Eeckhoute, J., Johnson, D. S., Bernstein, B. E., Nusbaum, C., Myers, R. M., Brown, M., Li, W., & Liu, X. S. (2008). Model-based Analysis of ChIP-Seq (MACS). *Genome Biology*, *9*(9), R137. https://doi.org/10.1186/gb-2008-9-9-r137

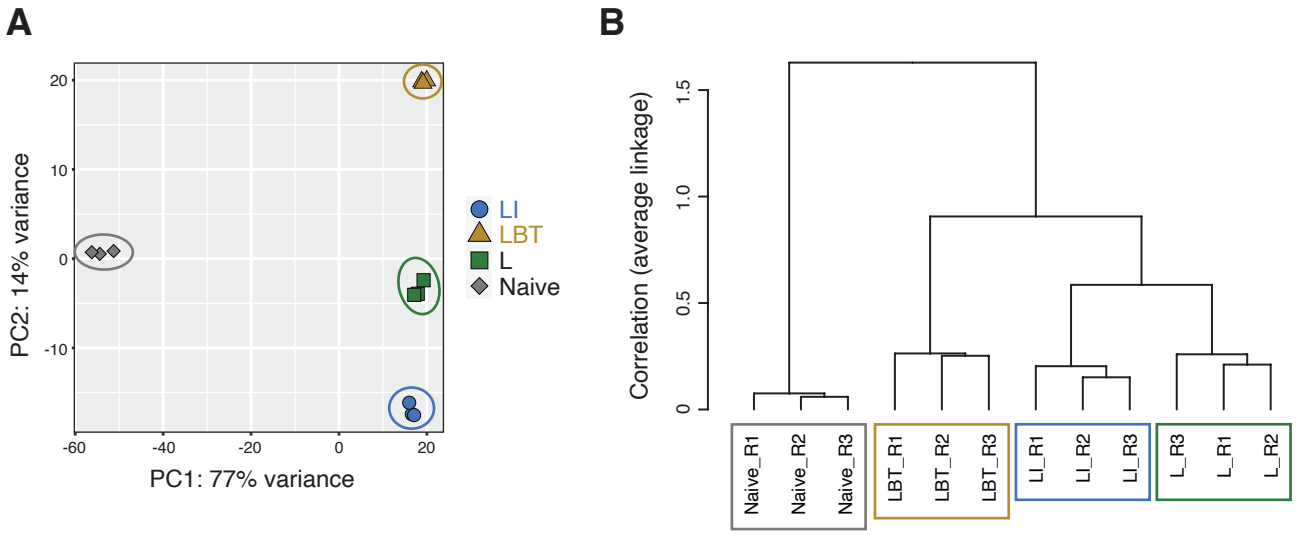

Figure S1. Stimulation-dependent clustering of B cell transcriptomics profiles after *ex vivo* activation. (A-B) Principal component analysis (A) and dendrogram (B) for the RNA-Seq datasets of WT splenocytes before (naïve) and after 48 h stimulation with LPS and IL-4 (LI), LPS, BAFF and TGFβ (LBT), or LPS only (L). The RNA-Seq analysis was performed on three biological replicates/mice per condition. Related to Figure 1.

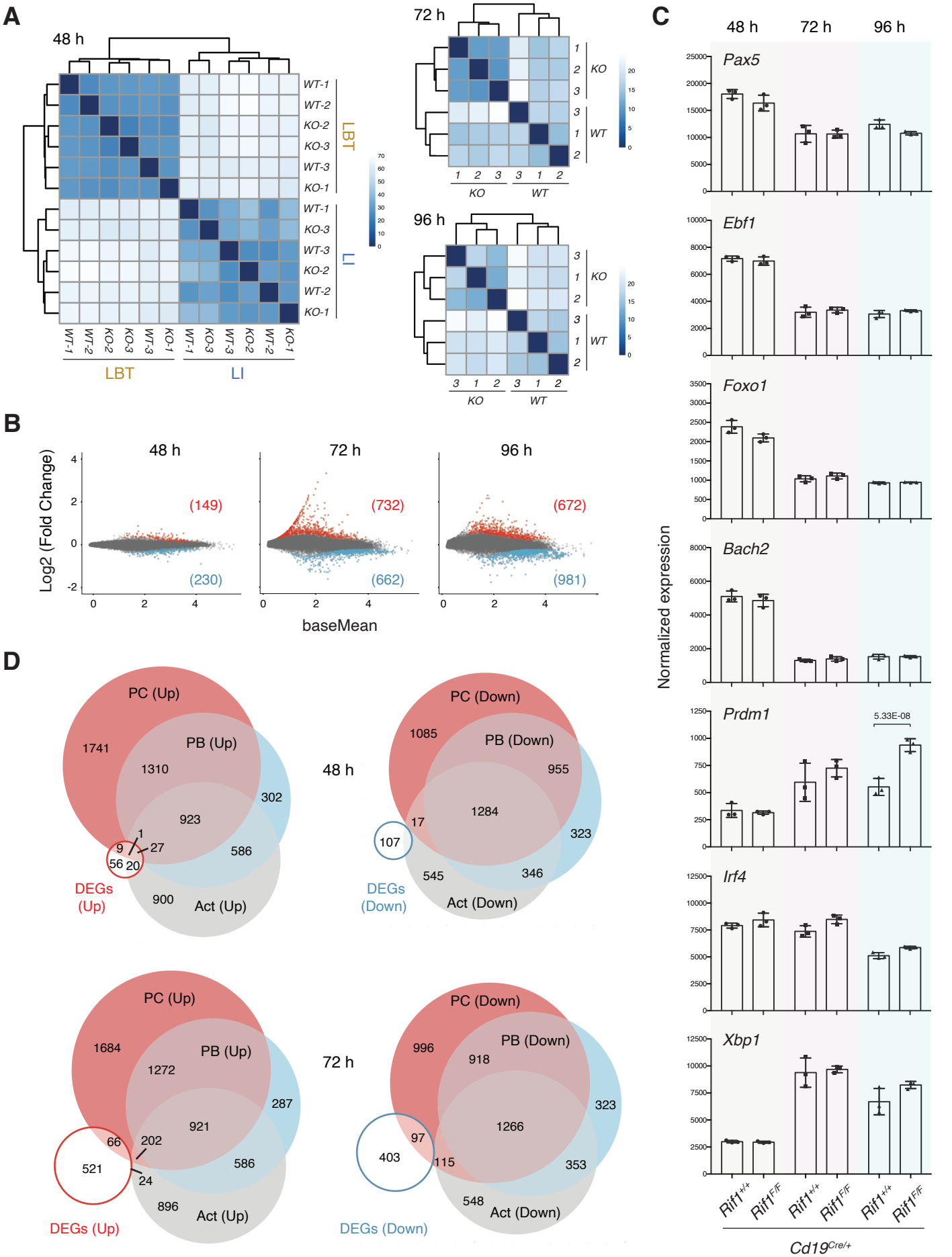
A
48 h
WT-1
WT-2
KO-2
KO-3
WT-3
KO-1
LBT
LI
72 h
96 h
KO
WT
B
48 h
72 h
96 h
Log2 (Fold Change)
(149)
(230)
(732)
(662)
(672)
(981)
baseMean
C
48 h
72 h
96 h
Pax5
Ebf1
Foxo1
Bach2
Prdm1
5.33E-08
Irf4
Xbp1
Normalized expression
Rif1+/+
Rif1F/F
Cd19Cre/+
D
PC (Up)
PB (Up)
Act (Up)
1741
1310
302
923
586
900
DEGs (Up)
48 h
PC (Down)
PB (Down)
Act (Down)
1085
955
1284
323
346
545
DEGs (Down)
72 h
1684
1272
287
921
586
896
521
66
202
24
996
918
1266
323
353
548
403
97
115

Figure S2. RIF1-deficiency alters the transcriptional landscape of activated B cells. (A-B) Dendrograms (A) and scatterplots (B) for the RNA-Seq datasets generated according to the experimental scheme depicted in Fig. 2A. For the 48 h time point, the analysis was performed on both LI- and LBT-stimulated cultures. Data summarizes results from three mice per genotype per stimulation condition. In the scatterplots, genes with an adjusted p-value <= 0.05 that are up- or down-regulated in *Rif1*$^{F/F}$*Cd19*$^{Cre/+}$ cells are highlighted in red or blue, respectively, and the number of DEGs per category is included in parenthesis. (C) Expression of *Pax5, Ebf1, Foxo1, Bach2, Irf4, Xbp1,* and *Prdm1* as determined by the RNA-Seq. Values were normalized by DESeq2 and the adjusted p-value of the only significant difference between samples is indicated. (D) Venn diagrams depicting the overlaps between genes up- (left) and down- (right) regulated in RIF1-deficient splenocytes at 48 h (top) and 72 h (bottom) post-activation and the corresponding up-and down-regulated (over naïve B cells) categories in the activated (Act) B cell, PB, and PC transcriptional signatures (Minnich et al. 2016). Related to Figure 2.

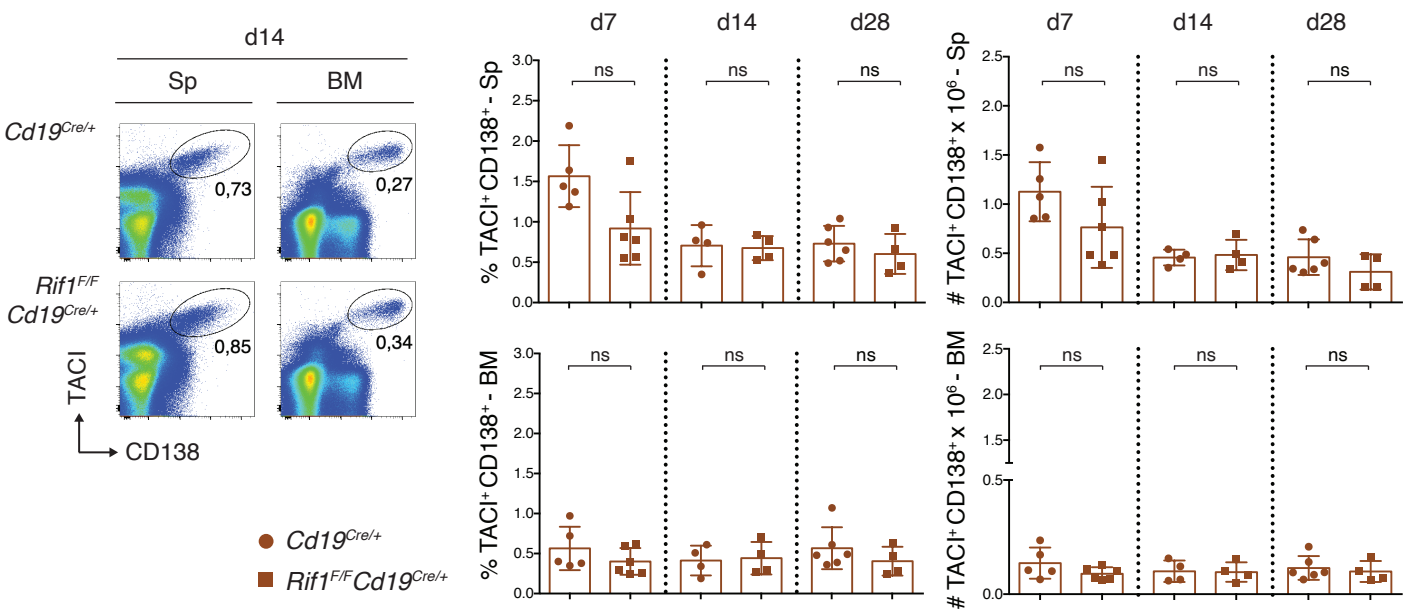

Figure S3. *Rif1*$^{F/F}$*Cd19*$^{Cre/+}$ mice exhibit physiological numbers of ASCs after immunization. Left: Representative flow cytometry plots measuring percentage and number of antibody secreting cells in spleens and bone marrows of mice of the indicated genotypes at day 14 after immunization, and according to the scheme in Fig. 4A. Right: Graphs summarizing the percentage and number of antibody secreting cells in spleens (top) and bone marrows (bottom) for at least four mice per genotype and time point. Significance was calculated with the Mann–Whitney U test, and error bars represent SD. ns: not significant. Related to Figure 4.

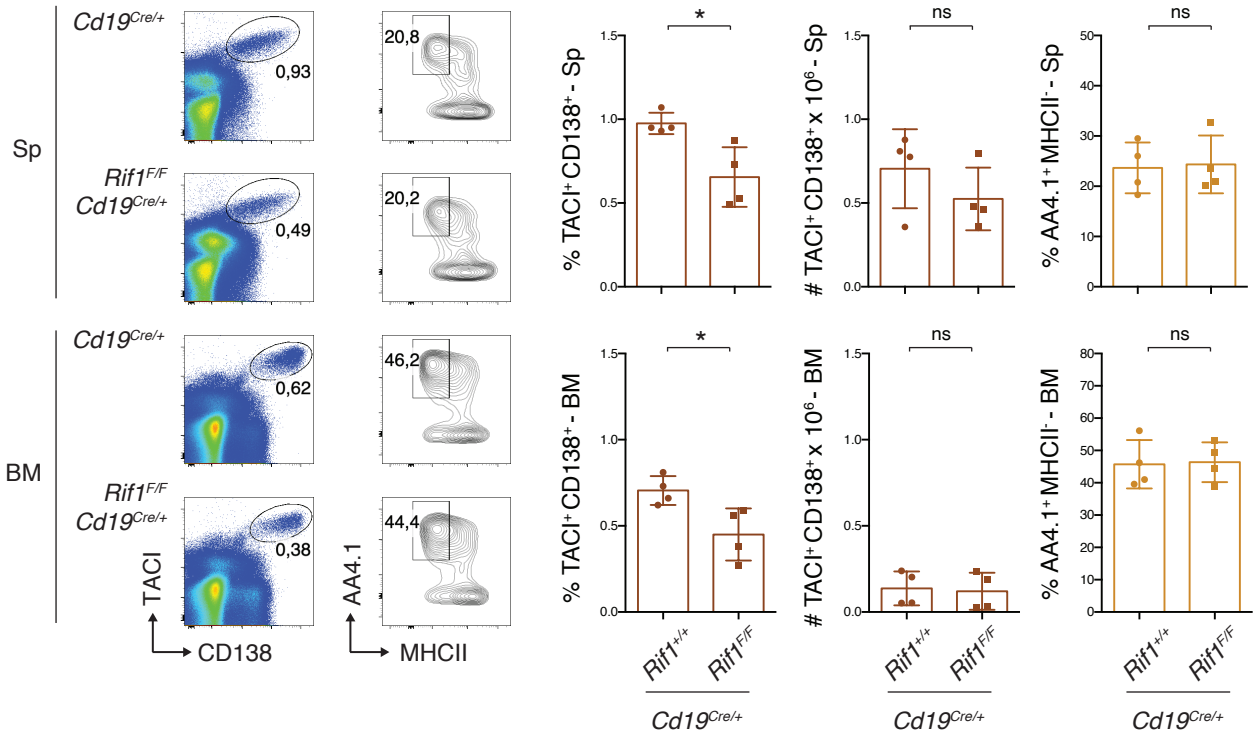

Figure S4. RIF1 ablation does not result in detectable changes of the plasma cell compartment in steady state condition. Left: Representative flow cytometry plots measuring percentage of antibody secreting cells and plasma cells in spleens and bone marrows of unimmunized mice of the indicated genotypes. The same gating strategy as in Figure 4A was employed. Sp: spleen; BM: bone marrow. Right: Summary graphs for four mice per genotype. Significance was calculated with the Mann–Whitney U test, and error bars represent SD. ns: not significant; * = $p \leq 0.05$. Related to Figure 4.

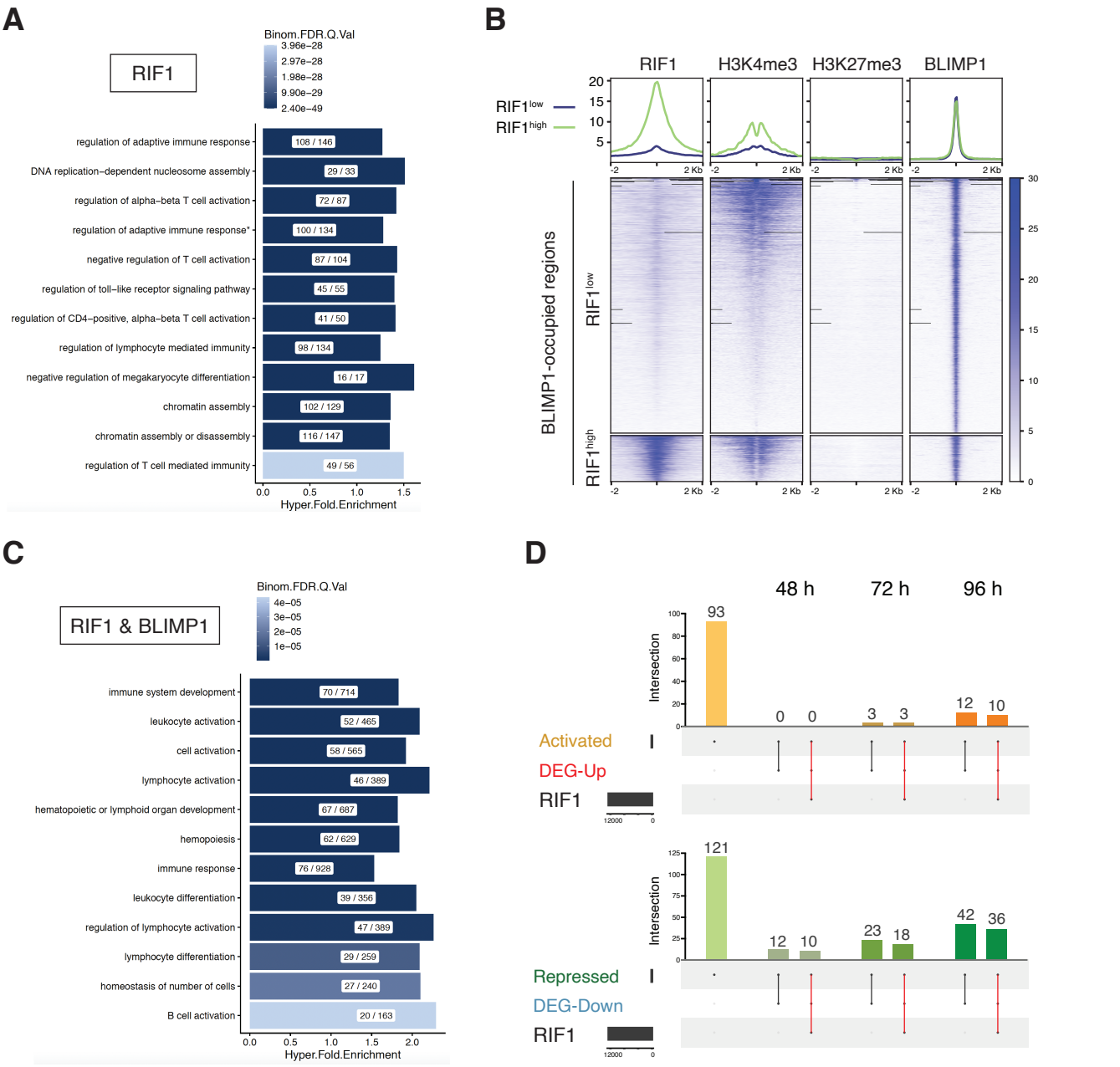

Figure S5. RIF1 and BLIMP1 co-occupied genomic regions comprise active genes involved in lymphocyte activation and differentiation. (A) Gene ontology enrichment analysis as determined by GREAT for the genomic regions bound by RIF1 in LI-stimulated B cells. The complete name of the category marked with " * " is "Regulation of adaptive immune response based on somatic recombination of immune receptors built from immunoglobulin superfamily domain". The X / Y ratio within each bar indicates the number of genes occupied by RIF1 (X) out of the total number of genes in the category (Y). FDR: false discovery rate. (B) Line plots (top) and heatmaps (bottom) depicting the comparative genome distribution of RIF1, H3K4me3, and H3K27me3 in reference to BLIMP1-occupied regions. The line plots illustrate the mean normalized signal distribution of the indicated proteins, whereas the heatmaps visualize their signal strength at each identified peak. The x-axis in both graph types represents the genomic region relative to the peak center. (C) GREAT gene ontology enrichment analysis of the genomic regions co-occupied by RIF1 and BLIMP1 in activated B cells. (D) UpSet plots depicting the intersection between activated BLIMP1 targets (Activated), genes differentially upregulated in *Rif1*$^{F/F}$*Cd19*$^{Cre/+}$ B cells (DEG-Up) and RIF1-occupied regions (top), and between repressed BLIMP1 targets (Repressed), genes differentially downregulated in *Rif1*$^{F/F}$*Cd19*$^{Cre/+}$ B cells (DEG-Down) and RIF1-occupied regions (bottom). The dot matrixes at the bottom of each graph show the intersection relationships among the data sets, with the number of common elements in the intersecting sets indicated above each bar. The red lines in the matrixes highlight the group of genes occupied and regulated by both BLIMP1 and RIF1. Related to Figure 5.